Available online at www.sciencedirect.com
SCIENCE DIRECT®
Journal of Power Sources 157 (2006) 114–120
JOURNAL OF POWER SOURCES
www.elsevier.com/locate/jpowsour

$Ru_xCr_ySe_z$ electrocatalyst for oxygen reduction in a polymer electrolyte membrane fuel cell

K. Suárez-Alcántara [a], A. Rodríguez-Castellanos [a], R. Dante [b], O. Solorza-Feria [a,*]

[a] *Depto. Química, Centro de Investigación y de Estudios Avanzados del IPN, A. Postal 14-740, 07360 México, D.F., México*
[b] *Depto. Ciencias Básicas, Tec de Monterrey, ITESM, Campus Ciudad de México, Calle del Puente 222, 14-380 México, D.F., Mexico*

Received 5 July 2005; accepted 27 July 2005
Available online 21 September 2005

Abstract

Powder of $Ru_xCr_ySe_z$ electrocatalyst was prepared from decarbonylation of the transition-metal carbonyl compounds in an organic solution containing dissolved selenium. The synthesized catalyst was characterized by FT-IR, X-ray diffraction (XRD), SEM and electrochemically. The powder catalyst presents high uniformity of cauliflower-like agglomerates of nanocrystalline particles embedded in an amorphous phase. The electrocatalysis of the oxygen reduction at this material on the ink-type electrode in acid electrolyte was studied by using the rotating disk electrode (RDE) technique. The $Ru_xCr_ySe_z$ catalyst presented attractive catalytic activity for the oxygen reduction reaction, ORR, in 0.5 M H_2SO_4. The Tafel slope for the ORR remains constant with temperature at -0.117 V dec^{-1} and the charge transfer coefficient increases in $d\alpha/dT = 1.8 \times 10^{-3}$, attributed to entropy turnover contribution similar to those reported on ruthenium-based selenide catalysts. The effect of temperature on the kinetics of ORR was analyzed and an apparent activation energy of 40.6 kJ mol^{-1} was determined. The performance achieved from the hydrogen–oxygen polymer electrolyte membrane fuel cell (PEMFC), with cathode of $Ru_xCr_ySe_z$ catalyst operating at different temperatures, was evaluated.

Keywords: Electrocatalysis; Oxygen reduction; Ru-based cluster catalyst; Membrane-electrode assembly; PEMFC

1. Introduction

Polymer electrolyte membrane fuel cells (PEMFCs) are considered as one of the most promising electrochemical devices for efficient generation of clean energy in the emerging hydrogen economy [1–4]. In order to improve the power density of PEMFCs, important issues, such as electrocatalytic activity of cathode electrodes and the essential properties of the membrane electrolyte, need to be addressed [5–7]. On the issue of increasing the electrocatalytic activity of the cathodic reaction in low temperature fuel cells, catalysts are usually based on highly dispersed nanoparticles of platinum and its alloy on an electronically conducting support. On the issue of increasing the electrocatalytic activity of the cathodic reaction, many catalysts have been synthesized and investigated in acid medium, and it has been found that Ru-based catalytic materials exhibit activity towards oxygen reduction reactions [8–10]. The higher electrocatalytic activity of these electrocatalysts can be achieved when bimetallic particles are synthesized in nanosized range [11,12]. The common approach adopted for the synthesis of the Ru-based catalysts include the decarbonylation of transition-metal carbonyl clusters compounds which are highly dispersed and supported in different substrates [13]. The reaction of these clusters with elemental chalcogenide generates a variety of polynuclear compounds with coordination center of d-states [14–16]. Oxygen reduction electrocatalysts which were prepared by chemical routes in non-aqueous solvent using organometallic precursors, achieve desired sizes of nanoparticles with homogeneous dispersion. Their electrocatalytical activity is carried out by a multielectron charge transfer process ($n = 4e^-$) to water formation. Hence, in order to produce desired sizes of novel nanoparticles, pyrolysis of transition-metal carbonyl compounds in organic solvent under refluxing condition is usually employed [17–19].

In the present work, the influence of the incorporation of chromium to Ru_xSe_z cluster nanocatalyst on the electrocatalysis of the ORR is investigated. The novel bimetallic chalcogenide electrocatalyst was produced through the decarbonylation reaction of ruthenium and chromium carbonyl compounds in sele-

* Corresponding author. Tel.: +52 55 5061 3715; fax: +52 55 5747 7113.
E-mail address: osolorza@cinvestav.mx (O. Solorza-Feria).

0378-7753/$ – see front matter © 2005 Elsevier B.V. All rights reserved.
doi:10.1016/j.jpowsour.2005.07.065

nium, dissolved in 1,6-hexanediol under refluxing condition for 2 h of synthesis at 220 °C. Well-dispersed nanoparticles of catalysts with about 5 nm in size were obtained, when Ru/Cr/Se molar ratio was fixed at 1:1:1. For electrochemical evaluation, the catalyst was ultrasonically mixed with Nafion ionomer and impregnated onto the electrode substrate. The linear sweep voltammetry investigation using a rotating disk electrode (RDE) shows that the oxygen reduction activity is fairly high compared to those obtained with Ru_x and Ru_xSe_y cluster compounds, previously reported [20,21]. The performance of a membrane-electrode assembly (MEA) in a single polymer electrolyte fuel cell is also presented, using $Ru_xCr_ySe_z$ cluster catalyst as a cathode electrode and Pt as an anode electrode.

2. Experimental

2.1. Catalyst synthesis

As described previously [11,21], nanometric ruthenium-based catalysts have been synthesized by pyrolysis of decarbonylation of transition-metal carbonyl compounds in organic solvent, under refluxing condition. The $Ru_xCr_ySe_z$ catalyst was synthesized by reacting 0.07 mM $Ru_3(CO)_{12}$ (Aldrich) with 0.20 mM $Cr(CO)_6$ and 0.20 mM of elemental selenium (Strem) in a chemical reactor containing 150 mL of 1,6-hexanediol (bp ≈ 220 °C at 585 mmHg), under refluxing condition for 2 h. After that, the chemical reactor was cooled down and a precipitated powder was recovered from the reaction medium with ethyl acetate and water. The resulting powder was washed ultrasonically with ethylic ether to eliminate organic reagents and to remove the non-reacted chemicals. The catalyst was dried for 24 h at room temperature. Afterwards, it was maintained in a closed recipient prior to utilization.

2.2. Chemical and physical characterization

In order to determine the peaks associated to remaining CO groups in the synthesized catalyst from those corresponding to carbonyls precursors, an infrared analysis in a air-dried KBr pellet was carried out, using a FT-IR Perkin-Elmer 16F spectrometer PC controlled. The surface morphology was examined using a scanning electronic microscope (SEM, FEI Sirion XL30) working at 5 kV. Phase identification was performed in the X-ray diffractometer for powders (Diffrac Bruker AXS, D8 Advanced Plus) operated at 30 mA and 35 kV using a monochromatic Cu Kα radiation, 1.54056 Å. XRD data were analyzed with the Diffrac Plus software and phase identification with the JCPDS data base.

2.3. Electrode preparation for RDE study and electrochemical set-up

In all the electrochemical studies, glassy carbon disks with a cross-sectional area of 0.07 cm^2 and thickness of 5 mm were used as a support for the thin films and used as working electrodes. Each disk was placed in a cup of an electrode holder made of Nylamid with a stainless steel bottom. Ink-type electrodes were prepared as follows: 1 mg of catalyst was added to an ethanol solution (40 μL) containing 10 μL of 5 wt% Nafion® (Du Pont, 1100 EW). The resulting mixture was sonicated for 2 min and 5 μL of catalytic ink was deposited onto the glassy carbon surface.

The electrochemical measurements were performed by using the conventional single compartment of a three-electrode test vessel. The cyclic voltammetry and the rotating disk electrode studies were performed in a potentiostat/galvanostat (EG&G Model 273A) and a Pine MSRX rotation speed controller. A platinum mesh was used as the counter electrode and Hg/Hg_2SO_4/0.5 M H_2SO_4 (MSE = 0.680 V/NHE) used as the reference electrode, placed outside the cell, kept at room temperature and connected by a porcelain Luggin capillary. All potentials are referred to NHE. The temperature of the cell from 298 to 333 K was controlled by a thermostat (Haake, Model F3). A 0.5 M H_2SO_4 electrolyte (pH 3) was prepared from doubly distilled water. Prior to electrochemical measurements the acid electrolyte was degassed with nitrogen for the working electrode activation. Thereafter, the acid electrolyte was saturated with pure oxygen and maintained during the electrochemical experiments. Hydrodynamic experiments were recorded in the rotation rate range of 100–2500 rpm at 5 mV s^{-1}.

2.4. Preparation and characterization of the membrane-electrode assembly

Catalytic inks were prepared by mixing and sonicating the electrocatalyst powder, Nafion solution and methanol; 10 wt% Pt/C from E-TEK (Electrochem) was used for the anode catalyst, and 10 wt% $Ru_xCr_ySe_z$/C catalyst was used for the cathode. Each MEA was prepared by spraying catalyst ink on each side of the pretreated Nafion 112 membrane. The load of catalyst at the anode and cathode was about 0.8 mg cm^{-2}. The MEA was prepared by placing the gas diffusion layer (carbon paper, Toray) above electrodes at both sides of the Nafion 112 membrane, followed by hot-pressing at 120 °C and 10 kg cm^{-2} for 1 min. The effective electrode area for the anode and cathode was 5 cm^2. The MEAs were tested with a commercial fuel cell system (Compucell GT, Electrochem) and a single cell rig with 5 cm^2 active geometrical area. The gas pressures at the anode and cathode were kept at 30 psi for H_2 and O_2, respectively. The fuel cell performance was measured from 25 to 80 °C, maintaining a flow rate of both gases of 550 cm^3 min^{-1}. Humidification of reactant gases was kept 5 °C above the temperature of the cell. Measurements were carried out under steady-state conditions.

3. Results and discussion

3.1. Catalyst characterization

The preparation of a Ru-based cluster catalyst by thermal condensation in organic solvent is not a selective synthesis, and a mixture of lower and higher nuclearity clusters is formed [22,23]. FT-IR spectra of a KBr pellet of the precursors and the powder catalyst of $Ru_xCr_ySe_z$ synthesized after 2 h of pyrolysis in 1,6-hexanediol was carried out.

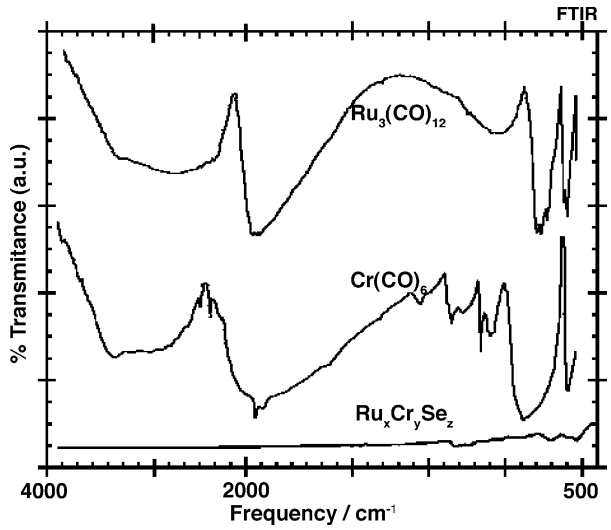

Fig. 1. FT-IR spectrum of $Ru_3(CO)_{12}$ and $Cr(CO)_6$ precursors to as-synthesized $Ru_xCr_ySe_y$ catalyst.

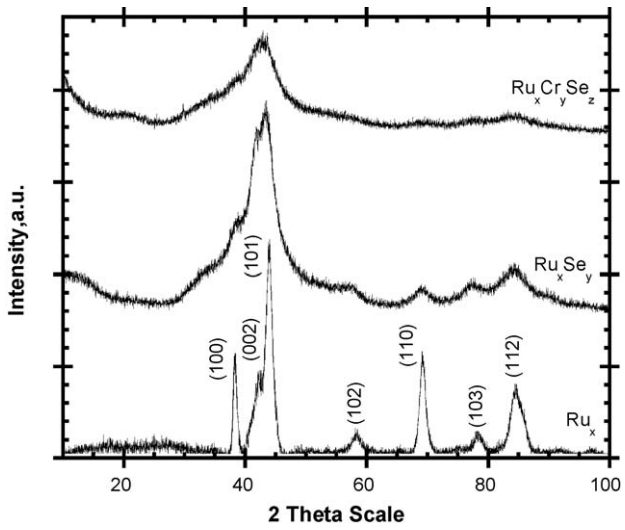

Fig. 3. XRD patterns of Ru_x, Ru_xSe_y and $Ru_xCr_ySe_z$ nanostructured catalyst as-synthesized in 1,6-hexanediol at 220 °C.

The FT-IR spectrum of the carbonyls precursors and the catalyst are shown in Fig. 1. The prominent band at around 2000 cm^{-1} corresponds to carbon monoxide stretching [(CO)-M] of the precursors ($Ru_3(CO)_{12}$ = 2054, 2016 and 1998 cm^{-1}, $Cr(CO)_6$ = 2000 cm^{-1}). After 2 h of reaction, all peaks of the bands disappear, indicating the completely thermal transformation of the terminal carbonyl groups of the precursors. This is evidence that in the chemical synthesis the M–CO bonds are destroyed.

The morphology of the as-synthesized powders of $Ru_xCr_ySe_z$ is displayed by the SEM micrograph in Fig. 2. The cauliflower-like image comprises agglomerates of clusters nanoparticles on the order of 100–150 nm in size. This range in size is common to ruthenium-based cluster catalysts synthesized in organic solvents [11,21] and the particle sizes suggest that this material could be a suitable candidate for use in electrocatalysis.

The X-ray diffraction (XRD) patterns of as-synthesized $Ru_xCr_ySe_z$ cluster catalyst compared with Ru_x and Ru_xSe_y, previously reported [11], is shown in Fig. 3. For all the samples, broad diffraction peaks indicative of the presence of nanocrystalline powders were observed. In the low angle scattering region a broad hump is observed suggesting that nanosized crystals may be embedded in an amorphous phase product. The pattern followed by $Ru_xCr_ySe_z$ catalyst suggests that the crystalline hexagonal ruthenium phase (JCPDS Card No. 6–663) is present as an important structure.

3.2. RDE study of oxygen reduction

The oxygen reduction reaction depends strongly on the hydrodynamic conditions. To study the kinetics of the oxygen reduction on a $Ru_xCr_ySe_z$ cluster catalyst ink-type electrode, a rotating disk electrode, RDE was used, immersed in oxygen

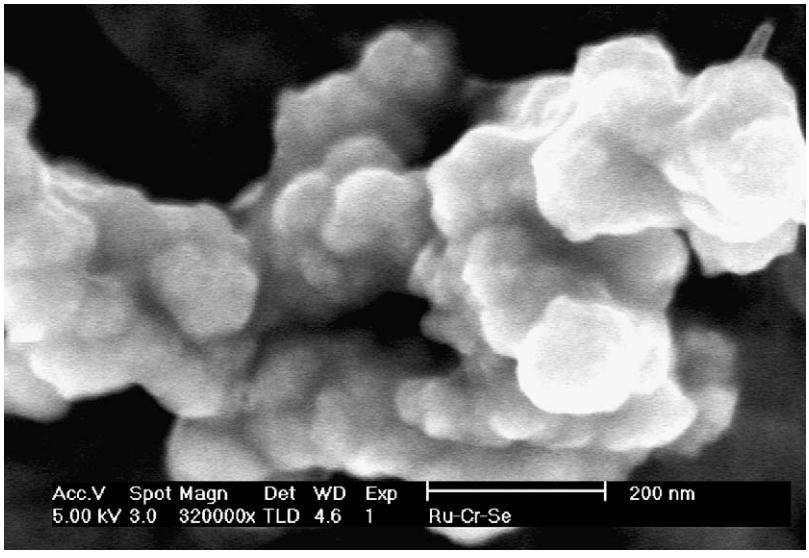

Fig. 2. SEM image of the $Ru_xCr_ySe_z$ cluster catalyst as-synthesized in 1,6-hexanediol at 220 °C.

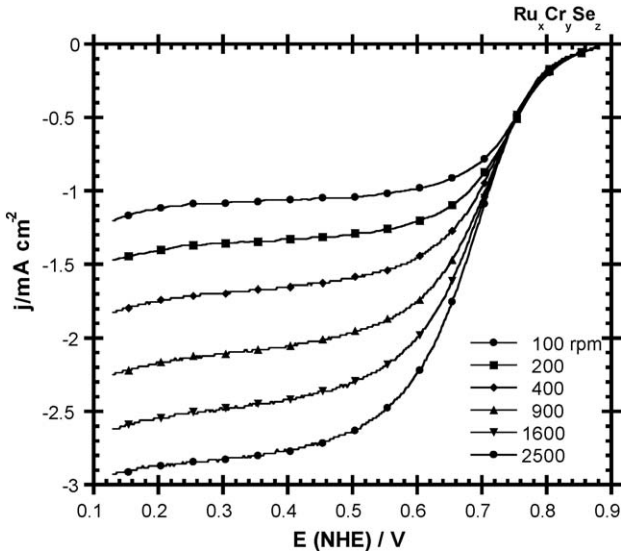

Fig. 4. Current–potential curves of oxygen reduction at $Ru_xCr_ySe_z$ cluster catalyst in 0.5 M H_2SO_4 saturated with oxygen at different rotation rates. Currents recorded at 5 mV s^{-1}.

saturated 0.5 M H_2SO_4, saturation being achieved by bubbling oxygen for 30 min. Prior to the electrochemical measurements, the electrode was activated by scanning the potential between 0.130 and 0.790 V V/NHE for 20 min in the outgassed acid electrolyte. Throughout the current–potential measurements, an oxygen atmosphere was maintained on the electrolyte surface. Fig. 4 shows the current–potential curves for the $Ru_xCr_ySe_z$ cluster catalyst for oxygen reduction obtained at various rotation rates, scanning the potential from the open circuit potential to 0.130 V/NHE at 5 mV s^{-1}. A charge-transfer kinetics control with rotation rate-independent current is observed in the range of 0.88–0.75 V/NHE, and at more cathodic potentials, mass transport became significant because of a well-defined transport-limited current dependence as a function of the rotation rate. A similar shape of polarization curve was observed for oxygen reduction on ink-type electrodes with a thin coat using ruthenium-based nanoparticles [23,24].

It was considered that increases in the limiting current are associated with the increase of oxygen diffusion through the electrode surface. In this electrocatalyst, the oxygen reduction is fast enough that at high overpotentials a flat limiting plateau is observed as for the Pt/C electrode [25]. An explanation of the current plateau could be the distribution of the electrocatalytic sites on the electrode surfaces. When distribution of active sites is less uniform and the electrocatalytic reaction is slower, the current plateau is more inclined.

In a film-coated electrode surface, the overall measured current, j, is related to the kinetic current, j_k, the boundary-layer diffusion-limited current, j_d, and film diffusion-limited current, j_f [26] by:

$$\frac{1}{j} = \frac{1}{j_k} + \frac{1}{j_d} + \frac{1}{j_f} \tag{1}$$

where j_f represents the film diffusion-limited current controlled by reactant diffusion in the Nafion® layer and is given by equation:

$$j_f = \frac{n_e F D_f C_f}{\delta_f} \tag{2}$$

In this equation, D_f and C_f are the diffusion coefficient and the concentration of O_2 in the film, respectively, and δ_f is the film thickness. The effect of the film diffusion is significant only in the case when the electrode is covered by a Nafion film [27] and can be neglected in the present study since the amount of Nafion (10 μL 5 wt% in 40 μL of solution) in the prepared catalyst suspension is sufficiently small and hence not expected to be a factor in the limiting current density on the rotating electrode, where only 5 μL of catalyst ink is loaded. The boundary-layer diffusion-limited current can be expressed as:

$$j_d = 0.2 n_e F C_o D_o^{2/3} \nu^{-1/6} \omega^{1/2} = B\omega^{1/2} \tag{3}$$

where 0.2 is a constant used, when ω is expressed in revolution per minute, n_e the number of electrons transferred per molecule of O_2 in the overall reaction, F the Faraday constant, C_o the concentration of oxygen dissolved (1.1×10^{-6} mol cm^{-3}), D_o the diffusion coefficient of oxygen in the solution (1.4×10^{-5} cm^2 s^{-1}), ν the cinematic viscosity of the sulfuric acid (1.0×10^{-2} cm^{-2} s^{-1}) [28] and B is the Levich constant. The current of the oxygen reduction reaction can be written as dependent on the kinetic current and the diffusion-limited current as shown in Eq. (4):

$$\frac{1}{j} = \frac{1}{j_k} + \frac{1}{j_d} = \frac{1}{j_k} + \frac{1}{B\omega^{1/2}} \tag{4}$$

From the data of Fig. 4, the Koutecky–Levich plots (j^{-1} versus $\omega^{-1/2}$) were drawn (Fig. 5). At all the rotation speeds, a series of essentially parallel straight lines in a broad potential range is illustrated in this figure, which indicates that the reaction order for the O_2 reduction at a $Ru_xCr_ySe_z$ cluster catalyst electrode is unity. Parallelism of the straight lines in Fig. 4 also indicates that

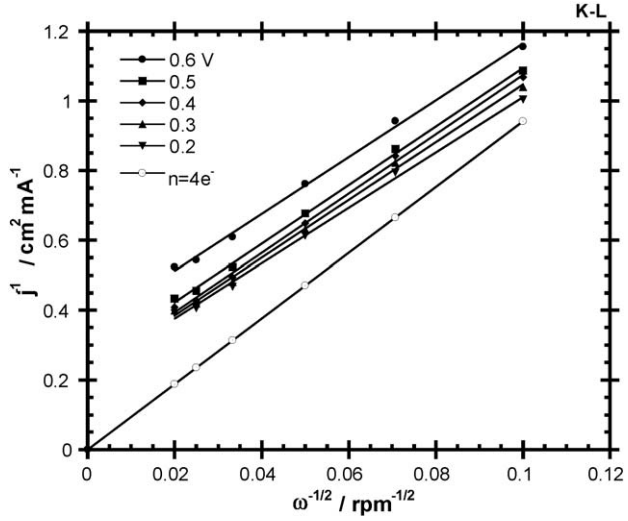

Fig. 5. Koutecky–Levitch plots for oxygen reduction on $Ru_xCr_ySe_z$ cluster catalyst ink-type electrode at different electrode potentials obtained from data of Fig. 3. Theoretical slopes for $n = 4e^-$.

the number of electron transferred per O_2 molecule and active surface area for the reaction not change significantly within the potential range studied. The experimental average slope value of those lines in Fig. 5 is 8.25×10^{-2} mA cm^{-2} rpm$^{-1/2}$, taking into account that the current density is related to the geometric area of the electrode surface. The theoretical slope calculated with the parameters described above for the transfer of four-electrons is 9.41×10^{-2} mA cm^{-2} rpm$^{-1/2}$. The behavior of the experimental and theoretical slopes is almost the same, although it should be noted that due to the uncertainly of the real area of the ink-type electrode, the number of electrons transferred per O_2 molecule could not be calculated precisely. From these results, we suggest that the O_2 reduction may proceed via the overall four-electron transfer reaction to water formation, i.e. $O_2 + 4H^+ + 4e^- \rightarrow 2H_2O$, as has been reported under the same experimental conditions for transition-metal chalcogenides cluster compounds [18,20,29].

Fig. 6 shows the mass transport corrected Tafel plots obtained for the $Ru_xCr_ySe_z$ cluster catalyst ink-type electrode on which oxygen reduction kinetics studies were conducted in 0.5 M H_2SO_4 at 298 K and at different temperatures. The Tafel plots were obtained after the measured currents were corrected for diffusion to give the kinetic currents in the mixed activation–diffusion region, calculated from Eq. (4):

$$j_k = j\frac{j_d}{j_d - j} \tag{5}$$

where $j_d/j_d - j$ is the mass transfer correction. The Tafel plots at all temperatures show a linear behavior in the mixed activation–diffusion region and a deviation of the kinetic current occurs with higher slope at high current density. As expected, the kinetics of the electrochemical reaction is higher at elevated temperatures, reflecting the temperature dependence of the chemical rate constant. A Tafel slope of -116.1 mV dec^{-1}, charge transfer coefficient of 0.51 and an exchange current density of 3.11×10^{-5} mA cm^{-2} was determined at 298 K. The kinetic

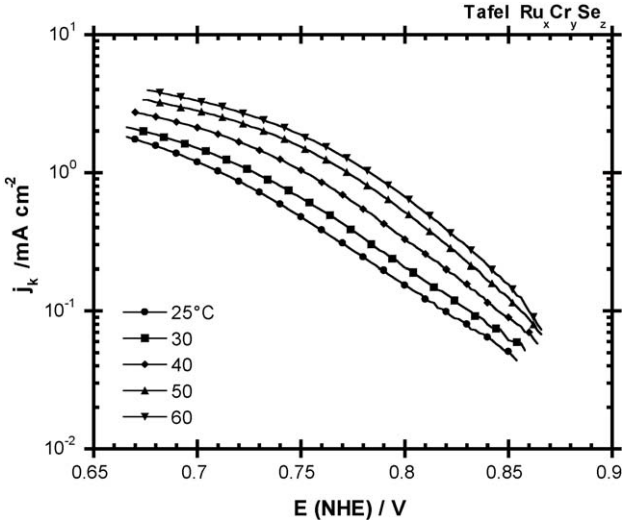

Fig. 6. Mass transfer corrected plots for oxygen reduction at a $Ru_xCr_ySe_z$ cluster catalyst ink-type electrode deposited in a glassy carbon, as a function of temperature.

Table 1
Effect of temperature on the kinetic parameters deduced from Tafel slope

T (K)	j_0 (mA cm^{-2})	b (mV dec^{-1})	α
298	3.11×10^{-5}	−116.1	0.51
303	4.69×10^{-5}	−117.1	0.51
313	8.34×10^{-5}	−117.3	0.53
323	1.25×10^{-4}	−115.9	0.55
333	1.79×10^{-4}	−115.6	0.57

parameters deduced for the oxygen reduction on $Ru_xCr_ySe_z$ cluster catalyst ink-type electrodes at different temperatures are presented in Table 1.

The effect of temperature on the kinetic parameters of the electrocatalyst is of paramount importance in the cathodic reaction of a fuel cell. The oxygen reduction was performed on a RDE by recording current–potential curves, similar to reported in Fig. 4, for each cell temperature. The mass transfer corrected current–potential curves at various temperatures are shown in Fig. 6. Effects such as the increase of the catalytic current and shift of the curves to more positive potentials were observed from increasing temperatures. This behavior is indicative of an enhancement of the electrocatalytic kinetic reduction of the adsorbed oxygen with temperature. To evaluate the exchange current density, j_o, and the charge transfer coefficient, α, from the Tafel slope as function of temperature, the dependence of the reversible oxygen electrode potential, E_r, on temperature [30] was evaluated using the value of ΔG° (H_2–O_2 cell) at each temperature using Eqs. (6a) and (6b):

$$\Delta G^\circ = [-70650 - 8T\ \ln T + 92.84T]\ \text{cal mol}^{-1} \tag{6a}$$

$$E_r = \frac{-\Delta G^\circ}{2F} \tag{6b}$$

Tafel slopes and kinetic parameters deduced from the linear part at each temperature of Fig. 6, are presented in Table 1. One can see that the Tafel slope is practically invariant with temperature, leading to a dependence of the transfer coefficient with temperature. Kinetic studies commonly assume that there are enthalpic, α_H and entropic, α_S contributions on the transfer coefficient [31,32], given by $\alpha = \alpha_H + \alpha_S T$. Table 1 shows Tafel slopes are invariant with temperature and are closely equal to 120 mV at all temperatures, i.e. to $2.3 \times 2RT/(\alpha_S TF)$. This invariance leads to $\alpha = \alpha_S T = 1.84 \times 10^{-3}$ T and $\alpha_H = 0$, deduced from the slope of a plot of α versus T shown in Fig. 7. Interestingly, the entropy transfer coefficient is the determining factor for the catalytic activity of the electrochemical reaction indicating that the entropy turnover plays one of the most important roles in the oxygen reduction reaction on the $Ru_xCr_ySe_z$ cluster catalyst. Similar results are reported at gold electrodes [31,33] and at nanoparticles of ruthenium in an acid electrolyte [21].

The exchange current density corresponding to each Tafel slope was calculated by extrapolating the potential to the E_r value at the experimental operating cell temperature. The temperature dependence of the exchange current density in Table 1 can be analyzed via conventional Arrhenius plot (Fig. 8). The apparent activation energy, $E^\#$, for the oxygen reduction reac-

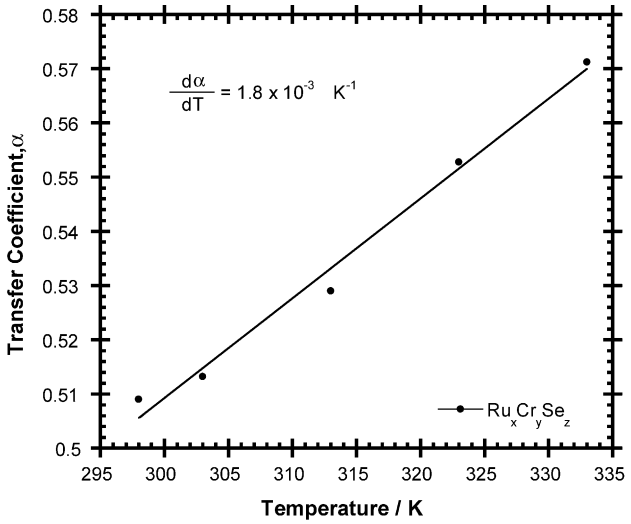

Fig. 7. Variation of the transfer coefficient for ORR in 0.5 M H_2SO_4, as a function of temperature.

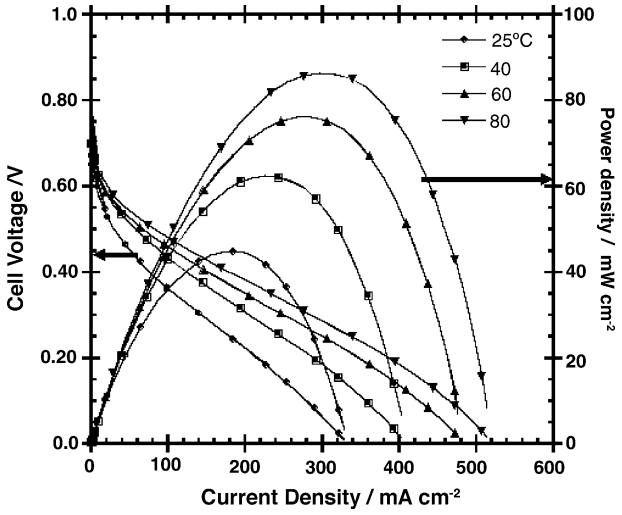

Fig. 9. Performance curves for Pt anode/$Ru_xCr_ySe_z$ cathode, operating on H_2/O_2 at 30 psi at different temperatures.

tion on $Ru_xCr_ySe_z$ cluster catalyst was calculated from a linear regression analysis of the slope of the Arrhenius equation represented by the relationship,

$$E^{\#} = -2.3R\left[\frac{\mathrm{d}\log i_o}{\mathrm{d}(1/T)}\right] \quad (7)$$

The apparent activation energy of 40.6 kJ mol^{-1} determined in 0.5 M H_2SO_4 lies in the range of 25–60 kJ mol^{-1} reported for other materials for the oxygen reduction in acid media [34,35]. One should keep in mind that the assessment of the activation energy at the reversible oxygen potential is only an estimate of the activation energy, i.e. $E^{\#}$ is the apparent activation energy.

3.3. Fuel cell performance

Fig. 9 shows the performance achieved at different temperatures, from 25 to 80 °C of a H_2/O_2, Pt (anode)/ $Ru_xCr_ySe_z$ (cathode) PEMFC. The assembly with $Ru_xCr_ySe_z$ was made using 0.8 mg cm^{-2} of the corresponding catalyst at 10 wt% in anode and cathode over Nafion® 115 polymer electrolyte membrane. The maximum power density (0.090 W cm^{-2}) achieved at 0.3 mA cm^{-2} is lower compared with typical Pt catalysts, however, we hope this value can rise by optimizing the assembly preparation. This initial test indicated that the system was limited by Ohmic losses and interfacial contact resistance. Our continued efforts focus on attempts to reduce these Ohmic losses in the construction process of assemblies and by integration of improved intrinsic properties of the $Ru_xCr_ySe_z$ catalyst by reducing the amorphous phase presented in the bimetallic chalcogenide material.

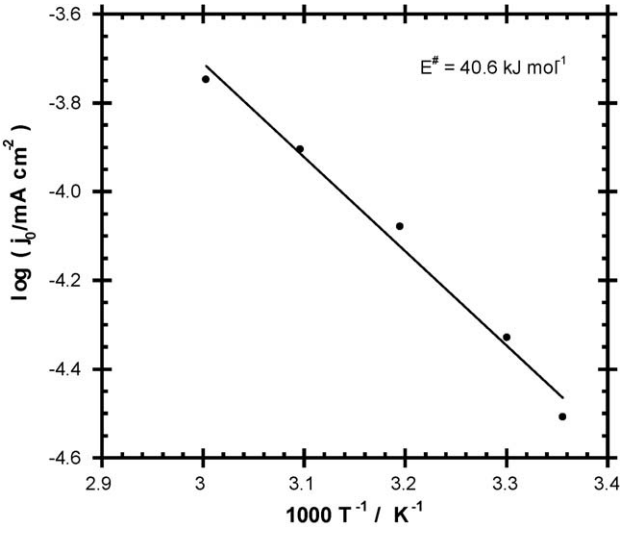

Fig. 8. Electrochemical Arrhenius plot for ORR in 0.5 M H_2SO_4.

4. Conclusions

$Ru_xCr_ySe_z$ cluster catalyst was synthesized in an organic solvent to be used as a cathode electrode in a polymer membrane fuel cell. This bimetallic chalcogenide catalyst presents high electrocatalytic activity for the oxygen reduction in acid electrolyte. From the RDE experiments, a multielectron charge transfer process ($n = 4e^-$) for the oxygen reaction was determined and an average Tafel slope of −116 mV dec^{-1} was obtained from the linear mixed activation–diffusion region in the range of temperatures analyzed. The transfer coefficient as a function of temperature denotes that the entropy turnover plays an important role on the ORR electrocatalytic process. The value of the apparent activation energy lies in the range of the reported results for other electrocatalysts for ORR in acid electrolyte [34]. The performance achieved by the H_2/O_2 PEM single fuel cell is related to the intrinsic properties of the $Ru_xCr_ySe_z$ catalyst and to the Ohmic losses and interfacial contact resistance created in MEA preparations, a situation which could be improved by increasing the crystalline phases of the catalyst and by optimizing catalysts loads and operating conditions.

Acknowledgments

This work was partially supported by a Grant of National Science and Technology Council of Mexico, CONACYT (Ref. 46094). One of the authors (K.S.A.) would like to thank CONACYT for providing her the doctoral fellowship. The authors thank to Dr. José Chavez and Dr. Gerardo Cabañas for assistance in XRD and SEM measurements.

References

[1] E. Antolini, J. Appl. Electrochem. 34 (2004) 563–576.
[2] V. Metha, J.S. Cooper, J. Power Sources 114 (2003) 32–53.
[3] L. Carrette, K.A. Friedrich, U. Stimming, Fuel Cells 1 (2001) 5–39.
[4] Y. Song, J.M. Fenton, H. Russel, L.J. Bonwille, M.V. Williams, J. Electrochem. Soc. 152 (2005) A539–A544.
[5] Ye Siyu, K.H. Vijh, J. Solid State Electrochem. 9 (2005) 146–153.
[6] M. Gattrell, B. MacDougall, in: W. Vielstich, A. Lamm, H.A. Gasteiger (Eds.), Handbook of Fuel Cells: Fundamentals Technology and Applications, vol. 2, John Wiley and Sons, 2003, pp. 443–464.
[7] J. Larminie, A. Dicks, Fuel Cell Systems Explained, John Wiley and Sons, 2000.
[8] M. Bron, P. Bogdanoff, S. Fiechter, I. Dorbandt, M. Schulenburg, H. Tributsch, J. Electroanal. Chem. 500 (2001) 510–517.
[9] T.J. Schmidt, U.A. Paulus, H.A. Gestaiger, N. Alonso-Vante, R.J. Behm, J. Electrochem. Soc. 147 (2000) 2620–2624.
[10] N. Alonso-Vante, H. Tributsch, O. Solorza-Feria, Electrochim. Acta 40 (1995) 567–576.
[11] R.G. González-Huerta, J.A. Chávez-Carvayar and O. Solorza-Feria, J. Power Sources, in press.
[12] R. Rivera-Noriega, N. Castillo-Hernández, A.B. Soto-Guzmán, O. Solorza-Feria, Int. J. Hydrogen Energy 27 (2002) 457–460.
[13] T.H. Walter, G.R. Frauenhoff, J.R. Shapley, E. Oldfield, Inorg. Chem. 27 (1988) 2561–2563.
[14] S.D. Rámirez-Raya, O. Solorza-Feria, E. Ordoñez-Regil, M. Benaissa, S.M. Fernández-Valverde, Nanostruct. Mater. 10 (1998) 1337–1346.
[15] E.W. Abel, F.G.A. Stone, G. Wilkinson, Comprehensive Organometallic Chemistry, vol. 7, Pergamon Press, 1995, pp. 683–960 (IIA, review 1982–1994).
[16] R.D. Adams, Polyhedron 4 (1985) 2003–2025.
[17] R.H. Castellanos, A. Campero, O. Solorza-Feria, Int. J. Hydrogen Energy 23 (1998) 1037–1040.
[18] O. Solorza-Feria, S. Citalán-Cigarroa, R. Rivera-Noriega, S.M. Fernández-Valverde, Electrochem. Comm. 1 (1999) 585–589.
[19] H. Yang, N. Alonso-Vante, C. Lamy, D.L. Akins, J. Electrochem. Soc. 152 (2005) A704–A709.
[20] R.G. González-Huerta, M.A. Leyva, O. Solorza-Feria, Rev. Soc. Quim. Mex. 48 (2004) 1–6.
[21] R.G. González-Huerta, R. González-Cruz, S. Citalán-Cigarroa, C. Montero-Ocampo, J. Chavez-Carvayar, O. Solorza-Feria, J. New Mater. Electrochem. Syst. 8 (2005) 15–23.
[22] D.M.P. Mingos, D.J. Wales, Introduction to Cluster Chemistry, Prentice Hall, Englewood Cliffs, NJ, 1990, pp. 32–40.
[23] R. González-Cruz, O. Solorza-Feria, J. Solid State Electrochem. 7 (2003) 289–295.
[24] S. Durón, R. Rivera-Noriega, P. Nkeng, G. Poillerat, O. Solorza-Feria, J. Electroanal. Chem. 566 (2004) 281–289.
[25] J. Murayama, I. Abe, Electrochim. Acta 48 (2003) 1443–1450.
[26] S.K. Zecevic, J.S. Wainright, M.H. Litt, S.L. Gojkovic, R.F. Savinell, J. Electrochem. Soc. 144 (1997) 2973–2982.
[27] N.M. Marcovic, H.A. Gasteiger, P.N. Ross Jr., J. Phys. Chem. 99 (1995) 3411–3415.
[28] K.-L. Hsueh, D.-T. Chin, S. Srinivasan, J. Electroanal. Chem. 153 (1983) 79–95.
[29] S. Durón, R. Rivera-Noriega, M.A. Leyva, P. Nkeng, G. Poillerat, O. Solorza-Feria, J. Solid State Electrochem. 4 (2000) 70–74.
[30] G. Lewis, M. Randall, International Critical Tables, vol. 7, McGraw Hill, NY, 1930, p. 232.
[31] A. Damjanovic, J. Electroanal. Chem. 355 (1993) 57–77.
[32] S.Lj. Gojkovic, S.K. Zecevic, D.M. Drazic, J. Electroanal. Chem. 399 (1995) 127–133.
[33] A.J. Appleby, J. Electroanal. Chem. 27 (1970) 325–334.
[34] K. Kinoshita, Electrochemical Oxygen Technology, Wiley, NY, 1992, pp.18–112.
[35] O. Solorza-Feria, S. Durón, Int. J. Hydrogen Energy 27 (2002) 451–455.